Gas-Phase Behavior of Galactofuranosides upon Collisional Fragmentation: A Multistage High-Resolution Ion Mobility Study

Simon Ollivier, Laurent Legentil, Oznur Yeni, Louis-Philippe David, Vincent Ferrières, Isabelle Compagnon, Hélène Rogniaux, David Ropartz

Gas-Phase Behavior of Galactofuranosides upon Collisional Fragmentation: A Multistage High-Resolution Ion Mobility Study

Simon Ollivier, Laurent Legentil, Oznur Yeni, Louis-Philippe David, Vincent Ferrie`res, Isabelle Compagnon, Hele`ne Rogniaux, and David Ropartz*

ABSTRACT: Carbohydrates are ubiquitous in nature but are among the least conserved biomolecules in life. These biopolymers pose a particular challenge to analytical chemists because of their high diversity and structural heterogeneity. In addition, they contain many isomerisms that complicate their structural characterization, notably by mass spectrometry. The tautomerism of the constitutive subunits is of particular interest. A given cyclized monosaccharide unit can take two forms: a most common 6-membered ring (pyranose, *p*) and a more flexible 5-membered ring (furanose, *f*). The tautomers impact the biological properties of polysaccharides, resulting in interesting properties of the derived oligosaccharides. From an analytical point of view, the impact of tautomerism on the gas-phase behavior of ions has scarcely been described in the literature. In this work, we study the behavior of Gal*f*-containing oligosaccharides, ionized as $[M+Li]_+$ species, under collisional dissociation (CID) conditions using high-resolution and multistage ion mobility (IMS) on a Cyclic IMS platform. In the first part of this work, we studied whether disaccharidic fragments released from Gal*f*-containing $(Gal)_1(Man)_2$ trisaccharides (and their Gal*p* counterpart) would match the corresponding disaccharide standards, and_despite the fragments generally being a good match_we showed the possibility of Gal*f* migrations and other unidentified alterations in the IMS profile. Next, we expanded on these unknown features using multistage IMS and molecular dynamics, unveiling the contributions of additional gas-phase conformers in the profile of fragments from a Gal*f*-containing trisaccharide compared with the corresponding disaccharides.

INTRODUCTION

Among other isomerisms of carbohydrates, furanose/pyranose tautomerism is particularly intriguing. This specific case of tautomerism consists of a given monosaccharide forming either a six-membered ring (pyranose) or a five-membered ring (furanose). In nature, hexoses and their derivatives most often adopt a pyranose configuration because it is more stable than the furanose form.[1] Yet there are some exceptions, notably with the occurrence of galactofuranose(Gal*f*)-containing polysaccharides. From a biological standpoint, it is interesting to understand why some organisms (including fungi, bacteria, and mycobacteria) biosynthesize hexoses in the form of five membered rings, which are not thermodynamically favored. In addition, there is increasing interest in finding new applications for carbohydrates, and Gal*f*-containing carbohydrates are no

exception to this general trend. Gal*f* has been reported across the tree of life in many harmless species/genera such as ***Penicillium***, ***Agelas*** (sponge), and ***Roccella*** (lichen) but also in highly infectious pathogens like ***Mycobacterium tuberculosis***, ***Trypanosoma cruzi***, and ***Shigella dysenteriae***.[2] For such pathogenic organisms, Gal*f*-containing components (including the biosynthetic pathways and involved enzymes) have been targeted to develop new therapeutic strategies.[3] However, a major obstacle to further exploitation and/or to better understanding of the biological role of Gal*f*-containing carbohydrates lies in the ability to accurately screen and identify such structures in biological matrices.

Mass spectrometry (MS) offers attractive characteristics to that aim, such as the sensitivity, the selectivity, and the quality of the structural information brought by MS and tandem MS experiments. However, the method alone is blind to many kinds of isomerisms, including furanose/pyranose tautomerism. Gas-phase methods that are sensitive to isomerism such as Ion Mobility-Mass Spectrometry (IMS-MS)[4–17] and InfraRed Multiple Photon Dissociation (IRMPD) spectroscopy[4,18–23] have been reported recently as promising complements to MS. In Favreau et al.,[4] both methods achieved a specific signature for Gal*p* or Gal*f* from a library of eight synthetic Gal-Man disaccharides, composed of all Gal*f*/Gal*p* pairs for the four linkage regioisomers of the Gal-Man linkage. This proof-of-concept work proposed that both IMS-MS and IRMPD could be considered to specifically detect Gal*f*-containing motifs in larger naturally occurring polysaccharides by using a bottom-up strategy involving fragmentation approaches such as CID (collision-induced dissociation). However, relatively few works have been conducted on the gas-phase behavior of furanosides upon slow thermal activation, such as CID or IRMPD, although this seems to be an important prerequisite to the validity of the previous strategy. Works by Schindler et al.[24] and Ho et al.[25] have studied the behavior of, respectively, Gal*f* NAc and Gal*f* compared to their pyranose counterparts using IRMPD spectroscopy. Questions remain, however, as to how furanosides, which are less thermodynamically stable than pyranosides, will behave upon slow thermal activation or whether specific rearrangements in the gas phase can be triggered by

activation.

In this study, we thus aimed at exploring in more depth the gas-phase behavior of Gal*f*-containing trisaccharides by means of ion mobility spectrometry (IMS). Briefly, IMS is a gas-phase method that separates ions according to their interaction with a buffer gas and an electric field; the resulting separation is ultimately related to the tridimensional structure of the ions. As detailed reviews are available elsewhere (see refs[26–28]), we will not detail all existing IMS methods here. However, one method of particular interest is Traveling Wave IMS (TWIMS) that separates ions using symmetric potential waves in a stationary gas, affording separations over long path length staying under the low-field limit. This is of notable interest because the resolving power (Rp) of TWIMS is a direct function of the square root of the ion path length. Extending the drift path length by cycling the ions for multiple passes around a racetrack has thus recently become a popular strategy to reach ultrahigh-resolution IMS, using Cyclic IMS (Waters Corp., Wilmslow, UK)[29] or Structures for Lossless Ion Manipulation (SLIM).[30] In particular, the Cyclic IMS (cIMS) technology is equipped with a multifunction array to redirect ions in a given direction affording multistage IMS (IMS_n) manipulations including precursor selection, collisioninduced dissociation, and IMS analysis of the fragments_ analogously to MS_n. This platform thus offers many advantages for the study of furanosides in the gas phase and was used in the present work to compare the fragmentation behavior of Gal*f*-trisaccharides to their Gal*p* counterparts.

To this end, we synthesized and analyzed galactomannan trisaccharides from two selected structural families of biological relevance. The first type of biologically relevant Gal-Man linkage consists of a Man-(*α*1,4)-Man backbone with branching of Gal*f* units in (*β*1,6). The Gal*f*-(*β*1,6)-Man*p* motif is notably found in symbiotic organisms (***Roccella decipens***, lichenized Ascomycete) but also in pathogenic organisms such as ***Aspergillus*** sp. and ***Paracoccidioides brasiliensis***.[2] The second type of selected Gal-Man linkage consists of a Man-(*α*1,6)-Man backbone with branching of Gal*f* units in (*β*1,4). Interestingly, the Gal*f*-(*β*1,4)-Man*p* motif is exclusively found in lichens but has been reported in various genera: ***Lasallia***, ***Gyrophora***, ***Usnea***, and ***Collema***.[31–35]

One additional challenge for such a study is that much of the work found in the literature regarding the fragmentation of oligosaccharides is studies conducted on protonated *N*-glycans. However, it is difficult to protonate neutral oligosaccharides that do not contain a nitrogen atom, and they are generally analyzed as alkali cation adducts (such as Li^+, Na^+, or K^+), both for MS and IMS analysis. This affords an easier separation of the ion populations in IMS.[36] Additionally, the interest of fragmentation approaches on alkali adducts has long been demonstrated, notably for the characterization of the linkage regioisomers.[37−39] Fragmentation studies performed in a preliminary work showed that, at an equivalent precursor dissociation rate, Li^+ adducts tend to give the best profiles in terms of fragment intensity, followed by Na^+, whereas K^+ gives little to no fragments (Figure S1). Therefore, the present study was conducted on Li^+ adducts. On the downside, documentation regarding the possible rearrangements occurring on Li^+ or Na^+ species is scarce, but such reports are increasing in the recent literature. For instance, Bythell and co-workers recently investigated the fragmentation pathways of alkali-cationized oligosaccharides using the Fafoom genetic algorithm and Density Functional Theory.[40,41] It is also notable that gasphase rearrangements of oligosaccharides that were previously considered impossible on alkali adducts, such as subunit migration and internal residue loss, were recently described for such ions.[42] This question whether other rearrangements described for protonated species can occur. For example, pyranose-to-furanose isomerization was recently evidenced in protonated peptidoglycans.[43,44]

EXPERIMENTAL SECTION

Synthesis of the Standards. ***Gal-Man Disaccharides.*** The Gal-Man disaccharides used as references in this study were previously used to build a library of IMS-MS and IRMPD profiles. Their synthesis and NMR validation are reported in this earlier publication by Favreau et al.[4]

Gal-Man-Man Trisaccharides. Gal-Man-Man trisaccharides were synthesized for this study using the approach fully described in another article to be published elsewhere.

Man-Man Disaccharides. Man-Man disaccharides were

also synthesized for this study to serve as references for the reducing end of the trisaccharides. Shortly, both mannobioses Man*p*-(1,6)-Man*p* and Man*p*-(1,4)-Man*p* were synthesized by coupling donor **1** to acceptors **2** and **3**, respectively, under acidic conditions. The resulting disaccharides were then submitted to standard deprotection steps under appropriate conditions to yield the desired disaccharides (Scheme 1).

Scheme 1. Principle of the Synthetic Way Used to Afford the Targeted Mannobioses

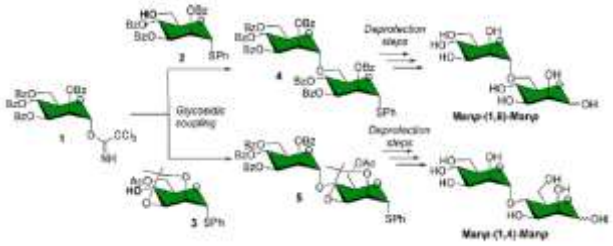

Further details about their synthesis and NMR validation are given in the Supporting Information.

^{18}O-Labeling of the Reducing End. A 50 μL portion of 1 mg/mL aqueous stock solution was speed-vacuum-dried and resuspended in the same volume of $H_2{}^{18}O$. Samples were incubated for 10 days at room temperature, away from light, to allow the mutarotation to exchange the hydroxyl group at the reducing end of the oligosaccharides.

Other Chemicals Used for IMS-MS Analysis. HPLCgrade methanol and acetonitrile were purchased from Carlo-Erba (Val de Reuil, France). Ultrapure water was produced by using a Milli-Q system (Millipore, Burlington, MA, USA). Lithium chloride (LiCl) and 97% $H_2{}^{18}O$ were purchased from Sigma-Aldrich (Saint Quentin Fallavier, France).

Cyclic IMS Analyses. *Analytical Conditions.* The analyses were performed on a SELECT SERIES Cyclic IMS (cIMS) QIMS-TOF spectrometer (Waters, Wilmslow, UK), with the TOF analyzer set to the sensitivity mode (V mode). Details about the voltages and pressures applied in the instrument are given in Supporting Text 1. Samples were infused at a concentration of 5 μg/mL in 50:50 water/methanol (v/v) at a flow rate of 5 μL/min. Lithium adducts were generated by

doping the solvents with 0.1 mM LiCl. To check the purity of the synthesized trisaccharides, the oligosaccharides were further analyzed using the HPLC gradients described in Supporting Text 2_all results presented in the main text were obtained in direct infusion. The trisaccharides were fragmented/activated using collision-induced dissociation (CID) either before IMS analysis (in the "trap" cell) or between two rounds of IMS (in so-called IMS/IMS experiments, see the next paragraph) using nitrogen as a collision gas. The choice of the fragmentation strategies is detailed throughout the description of the results.

Multistage IMS Experiments. IMS experiments were conducted at a pressure of 1.75 mbar in the ion mobility cell, with a traveling wave velocity of 375 m/s and a wave height of 22 V. The HR-IMS profiles of the disaccharides and disaccharidic fragments were acquired after a four-pass separation around the cyclic racetrack (17.5 ms of separation). Two types of multistage IMS experiments were further performed.

The first type of IMS^n experiment that was performed is the so-called "head-and-tail" or "top-and-tail" experiment (Figure S2). This experiment mainly serves the purpose of avoiding the wrap-around phenomenon. It is designed to specifically eject undesired ion populations_i.e., ions with higher or lower mobilities than the population of interest_from the ion mobility cell, before they have enough time to catch up to the desired population (for the faster ions) or before the population of interest catch them up (for the slower ions). By switching the multifunction array region in the "eject" direction, the undesired ions are ejected from the mobility cell, thus clearing the IMS range. This allows us to keep separating the populations of interest without being confronted by superimposition with the undesired population(s), which also makes this mode an interesting option to study the effect of extended exposure to the traveling waves. The main advantage of the "head-and-tail" experiment is that the ion population of interest stays in the racetrack while ejecting the undesired populations. Therefore, the separation that was already obtained for the species of interest is preserved and can be enhanced by additional passes.

The second type of IMS^n experiment_most useful for

structural characterization studies_is the “slicing” experiment (Figure S3). Like the “head-and-tail” experiment, it empties the mobility cell of the undesired ion populations, but opposite to the “head-and-tail” experiment, the ions of interest are sent backward in the prearray store cell (i.e., they do not remain in the cyclic racetrack). This is achieved by controlling the direction of the traveling wave in the multifunction array region (Figure S4A). Then, the ion population of interest is stored in the prearray store cell for an amount of time defined by the user, after which it can be reinjected in the cyclic IMS racetrack (Figure S4B). It is notably possible to activate/ fragment the selected population upon reinjection by increasing the reinjection voltages and making the ions collide with the IMS gas. In these experiments, fragmentation occurs at the entrance of the mobility cell, implying that CID is performed at IMS working pressure (1.75 mbar) instead of typical CID pressure (*ca* 2e-2 mbar). This makes fragmentation less effective and imposes a higher accelerating voltage.

IMS Data Processing. Data were processed using MassLynx 4.2 and Driftscope 2.9 (Waters, Wilmslow, UK). Drift times were recalculated from IMS arrival times by subtracting the times of all events preceding the final separation in the cIMS sequences. To correct for interday variability, the drift times were aligned using the disaccharide standards as a reference (these standards were analyzed in every analytical batch). The final drift time distributions (DTDs) of the disaccharides and disaccharidic fragments were then deconvolved with a Gaussian fitting strategy using CIUSuite2,[45] with expected peak widths of $0.6_0 \pm 0.1$ ms for Gal*f*-Man and Man-Man and of $0.5_8 \pm 0.1$ for Gal*p*-Man (detection up to >1% signal intensity, maximum number of peaks allowed = 6). All of the presented Gaussian deconvolutions exhibited R^2 scores ≥0.997. Collision cross section (CCS) calibration was performed using MajorMix (Waters, Wilmslow, UK) as an external standard using a logarithmic fit calibration method.[46,47]

Theoretical Studies on Man-(*α*1,6)-Man. *Molecular Dynamics.* Molecular Dynamics was used to explore the potential energy surface of complexes [Man-(*α*1,6)-Man*α* + Li]$_+$ and [Man-(*α*1,6)-Man*β* + Li]$_+$ with PM7 potential in

OpenMopac.[48] For each anomer, a trajectory of 10 ps at 1000 K was run and yielded 20 000 geometries. After optimization with PM7 and elimination of the identical conformers, around 4100 geometries were obtained for each anomer.

Theoretical CCS Calculations. Theoretical CCS values were calculated for representative conformations selected from the MD analysis of [Man-(α1,6)-Man + Li]$_+$ using IMoS Software v1.10. Calculations were performed using the Trajectory Method (4−6−12 Lennard-Jones-Induced Dipole model) for N_2 at a pressure of 175 Pa (1.75 mbar) and a temperature of 304 K. The default values for N_2 were applied for the other parameters (M_{gas} 28.00 Da, gas radius 1.5 A, polarization 1.7 A_3).

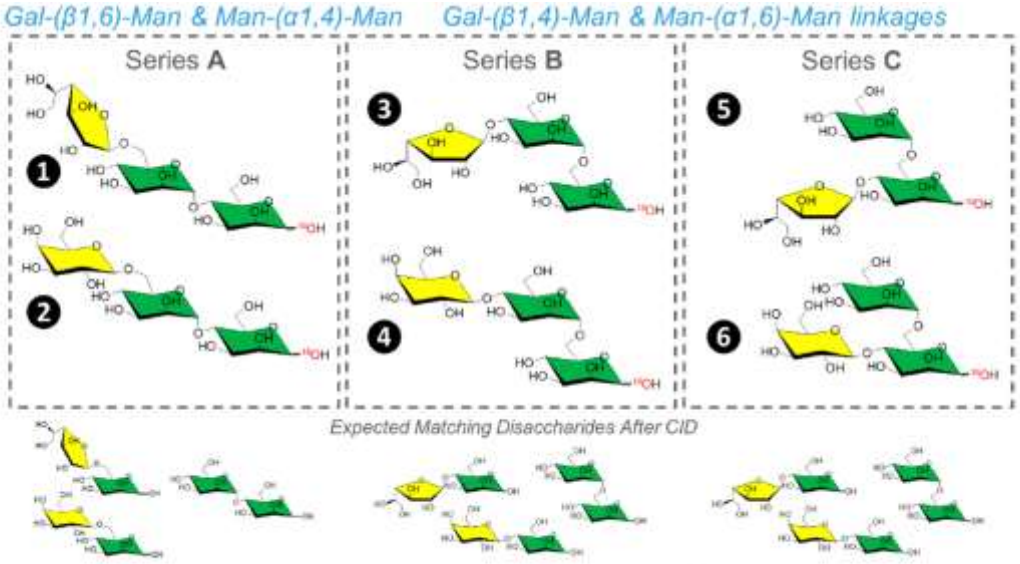

Figure 1. Galactomannan trisaccharides synthesized for CID-IMS analysis (labeled with ^{18}O at the reducing end) and expected matching disaccharides after CID for each series. Color code for the subunits: yellow = Gal, green = Man.

RESULTS AND DISCUSSION

Families of Considered Trisaccharides and Relevant Fragments. Galactomannan trisaccharides of the type $(Gal)_1(Man)_2$ selected from two structural families of biological relevance were considered in this study. They were chemically synthesized in their Gal*f* and Gal*p* forms alongside the corresponding Gal-Man and Man-Man disaccharides (Figure 1). They are divided into three series: Series A (trisaccharides ① and ②) represents the Gal-(β1,6)-Man + Man-(α1,4)-Man family, while Series B (trisaccharides ③ and ④) and Series C (trisaccharides ⑤ and ⑥) represent the Gal-

(*β*1,4)-Man + Man-(*α*1,6)-Man family.
Of note, the backbone of galactomannans is made of Man residues. Thus, Series A and B consist of “linear” trisaccharides, whereas in Series C the Gal residue is branched laterally on the reducing Man subunit. The odd-numbered species are Gal*f*containing trisaccharides, and even-numbered species are their Gal*p*-containing counterparts.

Does the IMS Profile of Disaccharidic Fragments Generated by CID Match the Corresponding Standards?

The initial hypothesis that drove our work was that ***the IMS profile of disaccharidic fragments should match the corresponding disaccharide references***. The three series of trisaccharides described above were used to test this hypothesis. We set up the cIMS separation of the reference disaccharides and disaccharidic fragments at four passes, which affords the separation of all reference disaccharides (10 isomers including Gal*f*-Man*p*, Gal*p*-Man*p*, and Man*p*-Man*p*, see Table S1) with the same parameters_whereas a higher number of passes would have required specific parameters for every disaccharide. Note that the number of passes influences the IMS profile by increasing the separation and that what appears to be a single peak at four passes may split into several at ultrahigh resolutions. For instance, reducing-end anomers of carbohydrates become separated at high IMS resolutions: Nagy et al. reported two peaks for reducing oligosaccharides using SLIM-IMS,[49] which was also observed by Ujma et al. using a cIMS and established to arise from the anomeric configuration of the reducing end.[12] Warnke et al. further validated this using a unique instrument coupling SLIM-IMS with cryo-infrared spectroscopy.[50]

Series A. The first selected series of trisaccharides consists of Gal*f*-(*β*1,6)-Man-(*α*1,4)-Man (compound ①) and its Gal*p*-(*β*1,6)-Man-(*α*1,4)-Man analogue (compound ②). Of note, LC-IMS-MS analysis of trisaccharide ① showed the presence in this sample of a contaminant of unknown nature (Figure S5), with a significant contribution to the MS signal of ca. 15% (Figure S6). Importantly, MS is not quantitative, and this does not reflect the actual purity of the sample, which was estimated to be greater than 95% using NMR spectroscopy. Because the contaminant can be partly resolved using cIMS (Figure S7), we thus analyzed Series A using slicing IMS/IMS that allows

discarding the contaminant from the IMS racetrack.
Trisaccharide ① was subjected to an energy of fragmentation of 150 eV upon reinjection from the prestore cell (a remaining contribution from the contaminant is possible, but it is reduced compared to trap fragmentation).
The IMS profiles of the disaccharidic fragments from trisaccharides ① and ② are compared to the corresponding reference disaccharides in Figure 2. The $_{18}$O-labeling of the reducing end allows us to distinguish the C_2 fragment coming from the nonreducing end (*m/z* 349) and the Y_2 fragment coming from the reducing end (*m/z* 351), as shown in Figure 2A. C and Y ions were considered rather than B and Z because they hold a water molecule and, therefore, are closer to the reference disaccharide structures to which we compare the mobility profiles of the fragments. When comparing IMS spectra, we consider the mobility profiles to be a good match if the number of peaks in the spectra and their drift times are comparable as well as the overall profile and peak shapes. It is noteworthy that the intensity of C_2 ions is always around 100-fold lower compared to the one of Y_2 ions when fragmenting oligosaccharides as $[M+Li]^+$ species using nitrogen as a collision gas. A remaining contribution of $_{16}$O-Y_2 in the IMS profile of C_2 is due to the remaining $_{16}$O (around 3%) in the $H_2{}^{18}O$ used for labeling.

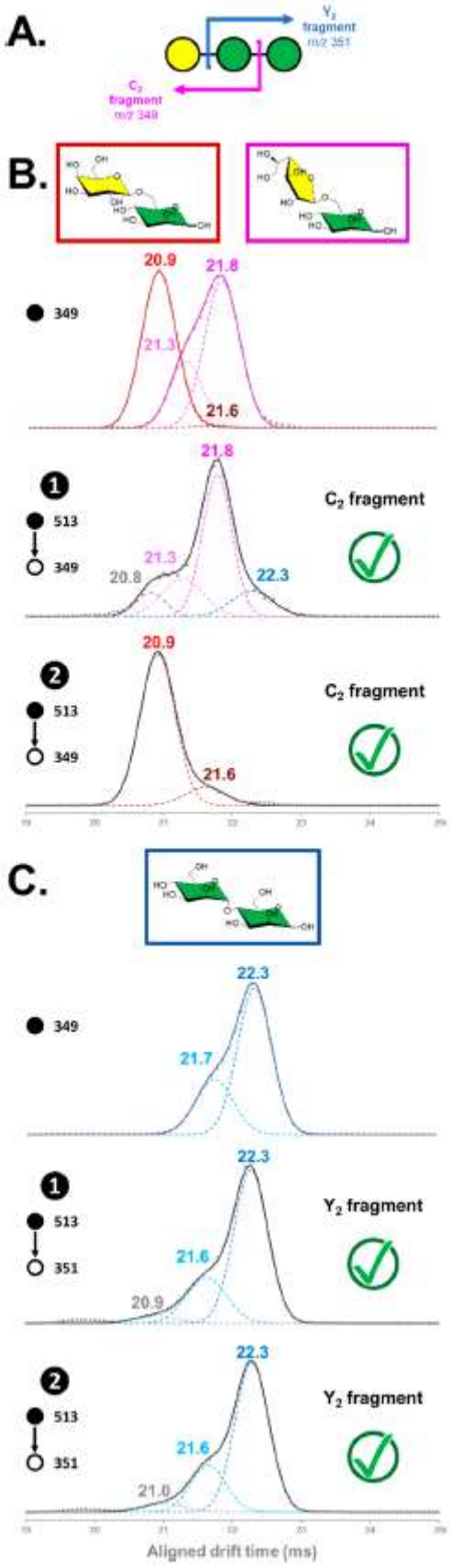

Figure 2. CID-IMS study of Gal-(β1,6)-Man-(α1,4)-Man trisaccharides (Series A). (A) Types of disaccharidic fragments formed from ^{18}O-labeled linear trisaccharides (nomenclature according to

Domon and Costello[51]). (B) Comparison of the C_2 fragments (m/z 349) from the nonreducing end of the trisaccharides to the reference unlabeled Galf/p-(β1,6)-Man disaccharides. (C) Comparison of the Y_2 fragments (m/z 351) from the reducing end of the trisaccharides to the reference unlabeled Man-(α1,4)-Man disaccharide. Dots: experimental data; solid line: global fit of the deconvolution; dashed lines: individual fitted gaussians.

Figure 2B presents the profiles of the Gal-(β1,6)-Man reference disaccharides compared to the C_2 fragments of trisaccharides ① and ②. The profile of Gal*f*-(β1,6)-Man exhibited two peaks at drift times of 21.8 and 21.3 ms (pink trace), while Gal*p*-(β1,6)-Man exhibited one major peak at 20.9 ms and a very minor peak at 21.6 ms (red trace, a *y*-axis zoom is presented in Figure S8). In the IMS profile of the C_2 fragment from trisaccharide ①, we observed four peaks: the two major ones at 21.8 and 21.3 ms corresponded, as expected, to the Gal*f*-containing disaccharide. We also observed a small contribution of ^{16}O-Y_2 at 22.3 ms, and the fourth peak with the lowest intensity was unidentified. However, this peak was absent when using the approach with an additional separation step in LC-IMS-MS (Figure S9), so we attributed it to a residual trace of the contaminant (see above). In the IMS profile of the C_2 fragment from trisaccharide ②, we observed two peaks at 20.9 and 21.6 ms, both matching those of the Gal*p*-containing disaccharide.
Figure 2C presents the profile of the Man-(α1,4)-Man disaccharide compared with the Y_2 fragments of trisaccharides ① and ②. The profile of the reference mannobiose (blue trace) exhibited two peaks with drift times of 22.3 and 21.7 ms. The Y_2 fragments of both trisaccharides presented, as expected, the same IMS profile, and these profiles were a good match to the reference disaccharide: two main peaks at 22.3 and 21.6 ms, and a third peak of lower intensity at 21 ms (possibly a minor conformation generated by the activation).
Overall, in the case of Series A, the IMS profiles of the disaccharidic fragments C_2 and Y_2 produced from Gal*f*- and Gal*p*-containing trisaccharides ① and ② were a good match to the fingerprints of the expected reference disaccharides, suggesting that the Gal*f*/Gal*p* isomerism is maintained upon

fragmentation.

Series B. We next selected a second type of trisaccharide with different branchings to check whether this Gal*f* resilience was always maintained. This series consists of Gal*f*-(*β*1,4)-Man-(*α*1,6)-Man (compound ③) and its Gal*p*-(*β*1,4)-Man-(*α*1,6)-Man analogue (compound ④). Contrary to Series A, Series B did not present any major contribution of contaminants in LC-MS analysis (some contaminants were present in ③, but none over 5% as shown in Figures S10 and S11), so we opted to perform CID in the trap cell with a collision energy of 50 eV, for a more efficient fragmentation and enhanced duty cycle. These linear trisaccharides give the same type of C_2 and Y_2 fragments as those in Series A (Figure 3A). The IMS profiles of the disaccharidic fragments from trisaccharides ③ and ④ are compared to the corresponding reference disaccharides in Figure 3.

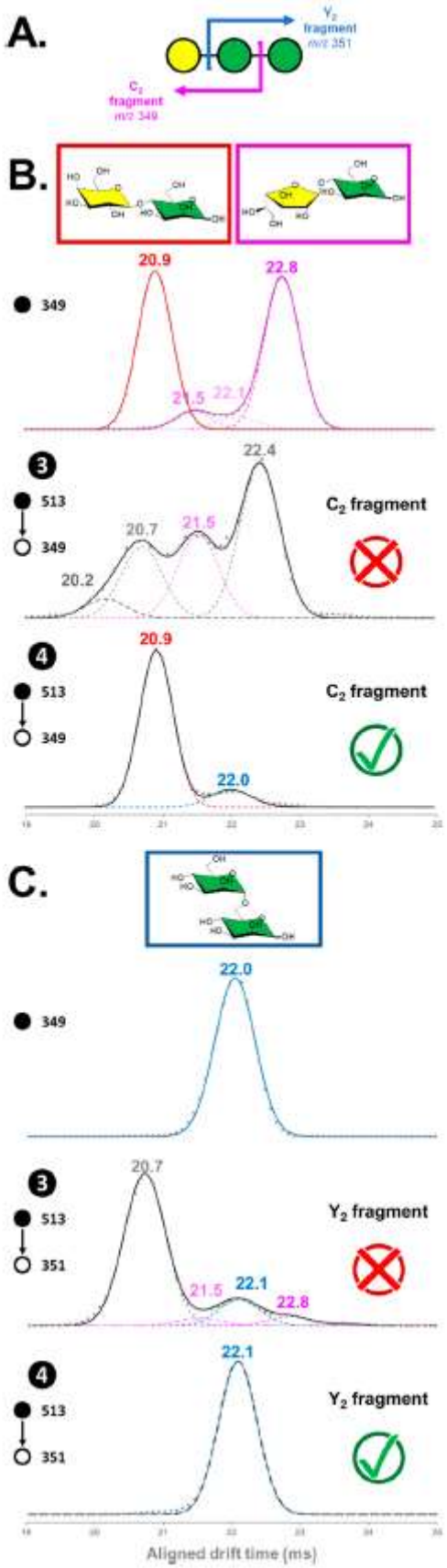

Figure 3. CID-IMS study of the Gal-(β1,4)-Man-(α1,6)-Man trisaccharides (Series B). (A) Types of disaccharidic fragments formed from ^{18}O-labeled linear trisaccharides (nomenclature

according to Domon and Costello[51]). (B) Comparison of the C_2 fragments (*m/z* 349) from the nonreducing end of the trisaccharides to the reference unlabeled Gal*f*/p-(*β*1,4)-Man disaccharides. (C) Comparison of the Y_2 fragments (*m/z* 351) from the reducing end of the trisaccharides to the reference unlabeled Man-(*α*1,6)-Man disaccharide. Dots: experimental data; solid line: global fit of the deconvolution; dashed lines: individual fitted gaussians.

Figure 3B presents the profiles of the Gal-(*β*1,4)-Man disaccharides compared to the C_2 fragments of trisaccharides ③ and ④. The profile of Gal*f*-(*β*1,4)-Man exhibited a major peak at a drift time of 22.8 ms and two minor peaks at 21.5 and 22.1 ms (pink trace), while Gal*p*-(*β*1,4)-Man exhibited a single peak at 20.9 ms after four passes of separation (red trace). In the IMS profile of the C_2 fragment from trisaccharide ③, only a single peak at 21.5 ms matched that contained in the profile of the reference Gal*f*-disaccharide. Otherwise, the profile also contained a feature at 20.7 ms (likely a ^{16}O contribution; see next paragraph) as well as two unidentified peaks at 22.4 (major) and 20.2 ms. This partial match could result from a greater flexibility of the furanose, but is difficult to investigate further because of very low signal intensity. On the other hand, the C_2 fragment of the Gal*p*-containing trisaccharide ④ matched well with the disaccharide standard, presenting a ^{18}O-labeled linear trisaccharides (nomenclature according to Domon and Costello[51]). (B) Comparison of the C_2 fragments (*m/z* 349) from the nonreducing end of the trisaccharides to the reference unlabeled Gal*f*/p-(*β*1,6)-Man disaccharides. (C) Comparison of the Y_2 fragments (*m/z* 351) from the reducing end of the trisaccharides to the reference unlabeled Man-(*α*1,4)-Man disaccharide. Dots: experimental data; solid line: global fit of the deconvolution; dashed lines: individual fitted gaussians.

major peak at 20.9 ms and a minor contribution of $^{16}O-Y_2$ at 22.0 ms.

Figure 3C presents the profile of the Man-(*α*1,6)-Man reference disaccharide compared to the Y_2 fragments of trisaccharides ③ and ④. The profile of the reference mannobiose (blue trace) exhibited a single peak after four passes of separation with a drift time of 22.0 ms. The Y_2 fragment of trisaccharide ③ exhibited an unexpected pattern: a main peak was observed at 20.7 ms, while the peak at the

expected drift time of Y_2 (22.1 ms) was minor. This peculiar behavior will be studied in more details in later sections of this article. In addition, we observed a doublet of peaks at 22.8 and 21.5 ms, which are specific of Gal*f*-(*β*1,4)-Man according to our disaccharide database,[4] that contains all regioisomers of Gal*f*-Man*p* and Gal*p*-Man*p* disaccharides (see Table S1). This indicates that in the case of trisaccharide ③ there has been a migration of the Gal*f* residue to C-4 of the reducing Man, with an internal residue loss of a Man subunit. This attribution was confirmed by comparing the MS_3 fragmentation pattern of the supposed rearrangement (refragmentation in the transfer cell of the IMS peak at 22.8 ms after IMS analysis) to the MS/MS spectrum of the Gal*f*-(*β*1,4)-Man disaccharide standard, as presented in Figure S12. Of note, only the IMS peak at 22.8 ms was resolved enough in the IMS dimension for MS_3 validation. It is noteworthy that the group of G. Glish has described a phenomenon of water adduction to lithium-cationized carbohydrates.[52–54] In this context, the MS_3 analysis also helped to exclude the possibility of the peak at 22.8 ms resulting from the contribution of a $[Z_2–Li_+–H_2O]_+$ adduct. This interpretation of the doublet at 21.5 and 22.8 ms being a migration of Gal*f* to C-4 of the reducing Man is finally supported by the fact that there is no apparent contamination of ③ by a trisaccharide, in which the Gal*f* residue is positioned on the reducing Man. Such a species was indeed included in the study and analyzed in Series C (species labeled ⑤) and was not detected in the LC-MS analyses of ③ (Figure S13). We observed that this Gal migration and the unknown feature seemed specific to Gal*f* because the Y_2 fragment of the Gal*p*containing analogue (trisaccharide ④) was a good match to the (*α*1,6)-mannobiose standard with a single peak at 22.1 ms. Overall, for Series B, we observed that the disaccharidic fragments were a good match to the corresponding reference disaccharides in the case of Gal*p*, but they were only a partial match for Gal*f*. Although we expected that there could be, to some extent, changes in the Gal*f*-containing C_2 fragments compared to those of the corresponding disaccharides, the discrepancy in the IMS profile of Y_2 ions (notably the main peak at 20.7 ms) was rather unexpected. Our hypothesis is that there is specific gas-phase behavior for Gal*f*-containing oligosaccharides with a possible migration of the Gal*f* subunit

to the reducing Man, as well as another parasitic phenomenon, which remained unidentified at this stage. Since this Y_2 fragment was produced with sufficient intensity, we decided to conduct further investigations.

Series C. Considering the unexpected behavior of trisaccharide ③, we first evaluated if a similar pattern would be observed for any trisaccharide containing this Gal*f*-(*β*1,4)-Man motif. We therefore synthesized and analyzed a new series of trisaccharides with the same type of linkages as Series B, but in which the Gal residue would be positioned on the reducing Man rather than at the nonreducing end. Series C thus consists of Man-(*α*1,6)-[Gal*f*-(*β*1,4)-]Man (compound ⑤) and its Man-(*α*1,6)-[Gal*p*-(*β*1,4)-]Man analogue (compound ⑥). These trisaccharides were analyzed using the same fragmentation method as that for Series B (CID in the trap cell at 50 eV).

The trisaccharides of Series C have a different fragmentation compared to Series A and B because both Gal and Man residues are branched on the reducing-end Man subunit. This results in Gal-Man (Y_1) and Man-Man (Y_α) disaccharidic fragments both containing ^{18}O and being observed at *m/z* 351 (Figure 4A). Of note, in the nomenclature we considered the Gal residue to be the lateral one because in galactomannans the backbone is made of Man while the Gal subunits are in lateral positions.

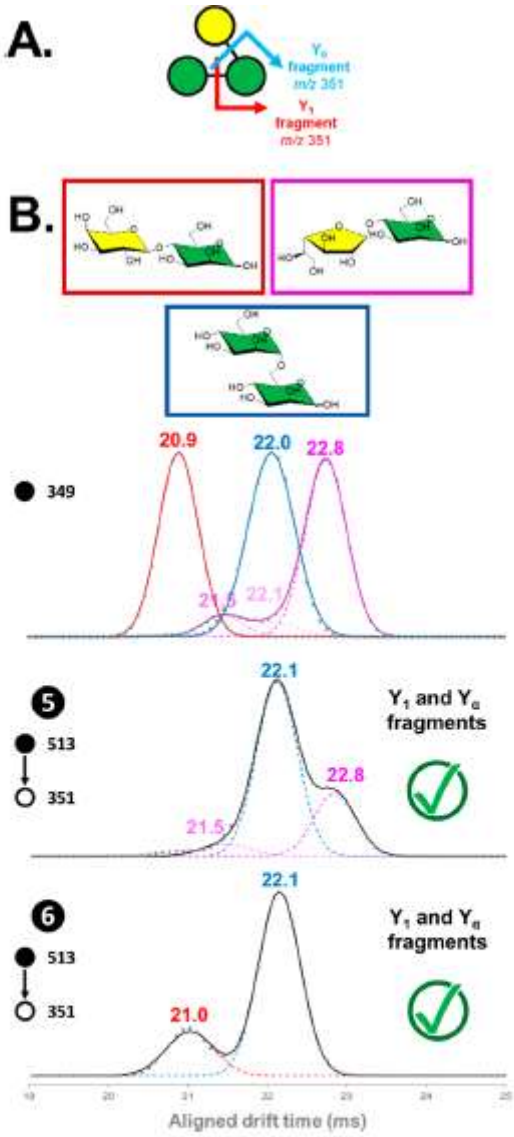

Figure 4. CID-IMS study of the Man-(α1,6)-[Gal-(β1,4)-]Man trisaccharides (Series C). (A) Types of disaccharidic fragments formed from ^{18}O-labeled branched trisaccharides (nomenclature according to Domon and Costello[51]). (B) Comparison of the Y_1 and Y_α fragments of the trisaccharides (both containing the reducing end at m/z 351) to the reference unlabeled Galf/p-(β1,4)-Man and Man-(α1,6)-Man disaccharides. Dots: experimental data; solid line: global fit of the deconvolution; dashed lines: individual fitted gaussians.

Figure 4B presents the results of the fragmentation experiments for trisaccharides ⑤ and ⑥. The profiles of the corresponding disaccharides are given for reference on the top trace and are identical with that described in Figure 3. In the profile of the disaccharidic fragments generated by CID of compound ⑤, we observe three peaks. The first had a drift time of 22.1 ms, matching the expected Y_α fragment. The other two peaks, at 22.8 and 21.5 ms, actually correspond to the expected values for the Gal*f*-containing Y_1 fragment. Regarding

compound ⑥, we observed two peaks: one at 22.1 ms that corresponds to Y_{α} and one at 21.0 ms that corresponds to the Gal*p*-containing Y_1 fragment.
Overall, for Series C, both Gal*f*- and Gal*p*-containing trisaccharides exhibited fragmentation profiles that matched very well with those of the corresponding disaccharides. This suggests that the behavior of compound ③ under CID conditions is not purely related to the presence of Gal*f* but might arise from its positioning at the nonreducing end and/or the regiochemistry of the mannose backbone in (*α*1,6).

In-Depth Investigation of the Gas-Phase Behavior of Trisaccharide ③ upon CID. We focused our interest on the major peak observed at a drift time of 20.7 ms on the IMS profiles observed for the Y_2 fragment produced from trisaccharide ③. In fact, when this peak was submitted to a further step of CID after IMS separation, it exhibited a pattern of cross-ring fragments typical of a (1,6) linkage (Figure S14), but it was absent from our database of drift times for reference disaccharides.
Initially, we suspected that this peak might be generated by inappropriate MS analysis conditions and performed several experiments to exclude this possibility. First, we performed an energy-resolved IMS (ER-IMS) experiment (Figure 5), showing that this peculiar profile was generated independently from the collision energy in the trap cell. This indicates either that a single dissociation pathway produces all species and that the lowest energy formable products are in equilibrium or that a general dissociation mechanism exists with multiple kinetically highly similar pathways.

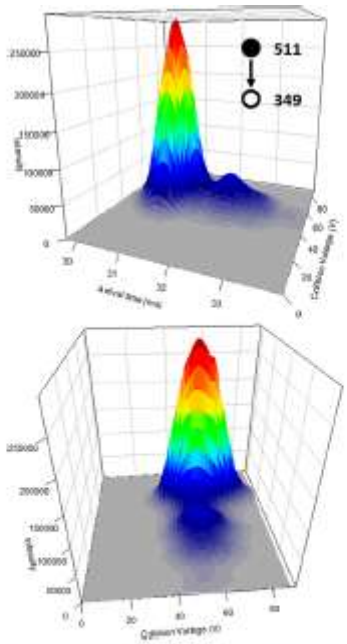

Figure 5. Energy-resolved IMS (ER-IMS) profile of the Y_2 fragment from trisaccharide ③ (two viewpoints of the same ER-IMS profile are presented for the sake of clarity). The oligosaccharide was analyzed in its unlabeled form (^{16}O at the reducing end, Y_2 at m/z 349) to avoid any back exchange with the solvent during the analysis.

Next, we assessed if the observation of an IMS peak at a shorter drift time was specific of the Li_+ adduct and if using another metal would impact the dissociation chemistry. We thus changed the countercation and analyzed trisaccharide ③ as $[M + Na]_+$ (*m/z* 529), but its Y_2 fragment (*m/z* 367) also had higher mobility compared to the (*α*1,6)-mannobiose standard (Figure S15). Finally, since we had observed a migration of the Gal*f* to C-4 of the reducing Man (Figure 3C, Y_2 fragment of trisaccharide ③, peaks at 21.5 and 22.8 ms), we considered that the feature at t_d 20.7 ms could be a migration of the Gal*f* to C-1 ((1,1)-linked disaccharides are absent from our database, and (1,1) linkages can give similar cross-ring fragments compared to (1,6) linkages). We thus analyzed an analogue of trisaccharide ③ protected in C-1 with a thiophenyl group that prevents migration to C-1 (assuming that the thiophenyl group has no major impact on the dissociation chemistry). Similar to trisaccharide ③, the Y_2 fragment generated from the C-1-blocked analogue also exhibited higher mobility compared to the corresponding protected disaccharide (Figure S16). This led us to conclude that the IMS peak at a shorter drift time in the Y_2 fragment of trisaccharide ③ is not a migration to C-1 of

the reducing Man subunit. Overall, these experiments confirmed that the compaction leading to the peak observed at t_d 20.7 ms occurred with different metals and was not a structural rearrangement, therefore hinting instead toward the existence of conformers of the Y_2 fragment of trisaccharide ③.

Gas-Phase Evidence for a Conformational Switch upon Collisional Activation. The above experiments ultimately led us to think that the presence of Gal*f* at the nonreducing end had an impact on the conformation of the parent trisaccharide. More specifically, at the level of the Y_2 fragment, the Man-(α1,6)-Man could be subject to a conformational switch because of the high degree of liberty of the (1,6) linkage. A detailed study of the IMS profile of (α1,6)-mannobiose (Figure S17) indeed revealed a slight shoulder at around 20.7 ms but that it was of very low intensity (below the detection threshold of CIUSuite for Gaussian fitting). However, the intensity of this shoulder could be enhanced with harsh CID conditions (fragmentation with a trap collision energy of 55 eV, i.e., 20 eV above our usual fragmentation parameters for disaccharides), which supported the idea that this peak could be a gas-phase conformer of (α1,6)-mannobiose. Similarly, the peak at 20.7 ms in the fragmentation profile of trisaccharide ③ could be a conformer of the expected Y_2 fragment found at 22.1 ms. A series of IMS/IMS experiments were thus conducted on both peaks of the fragmentation profile of trisaccharide ③ to verify whether the conformational switch between the two could be induced in the gas phase (Figure 6).

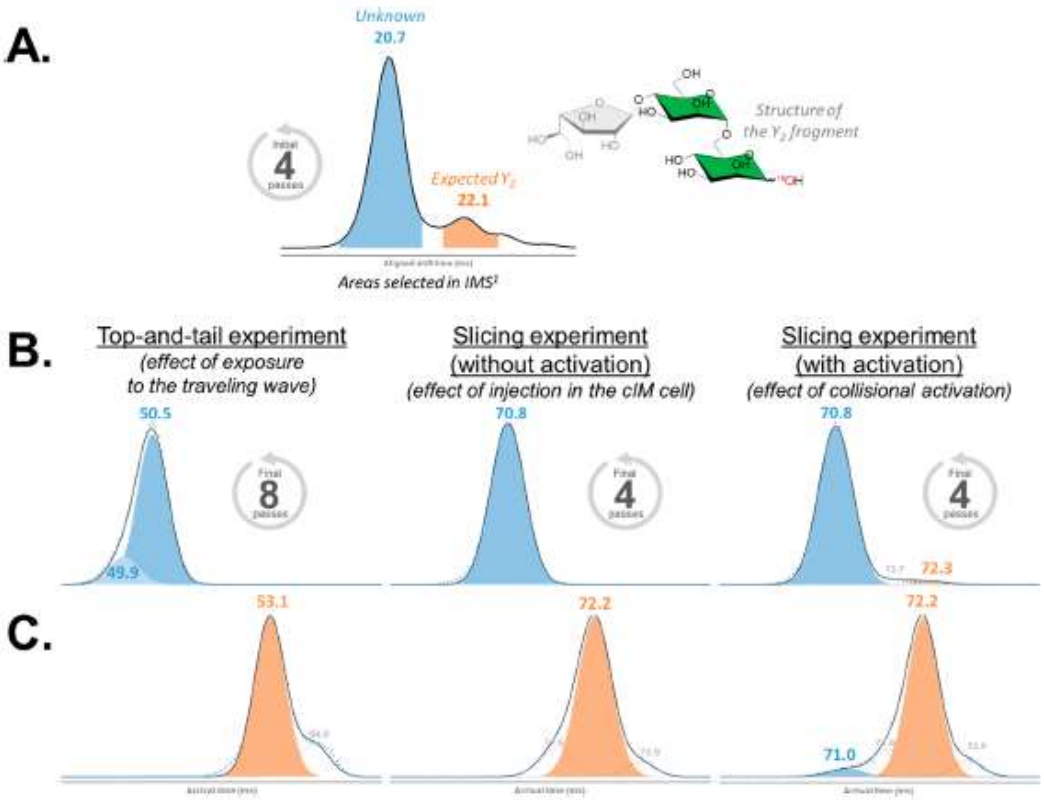

Figure 6. IMS^n investigation of the interconversion between the expected Y_2 fragment of trisaccharide ③ (t_d = 22.1 ms) and the unknown peak at t_d = 20.7 ms. (A) Structure of the Y_2 fragment and areas selected in IMS^1 for further analysis of the unknown peak (blue, main peak) and of the expected peak (orange). (B) Study of the peak at t_d = 22.1 ms (unknown) under different IMS^2 conditions. (C) Study of the peak at t_d = 20.7 ms (expected value for Y_2) under different IMS^2 conditions.

First, we performed a top-and-tail IMS/IMS experiment to study the effect of increased exposure to the traveling wave of the IMS cell. We doubled the time of exposure (i.e., performed an additional four passes), but we did not observe any interconversion between the two populations. However, this experiment unveiled that the peak observed at a drift time of 20.7 ms after four passes actually contains (at least) two peaks, observed here at arrival times of 49.9 and 50.5 ms.

Second, we moved to slicing IMS/IMS experiments, in which we ejected the populations of interest back to the prestore cell, then reinjected them and performed a new 4-pass separation. We reinjected the species from the prestore either without or with energy (100 eV) to activate them. Without energy, we did not observe an interconversion, showing that the transition between the rest of the spectrometer and the higher pressure of the IMS cell had no effect. In contrast, under activating conditions, we observed a conformational switch with the appearance of a peak at t_d 72.2 ms when isolating the peak of unknown origin (Figure 6B, right) and the appearance of a peak at t_d 70.9 ms when isolating the expected Y_2 peak

(Figure 6C, right). This shows that the conformational switch can be triggered by collisional activation.

In summary, we were able to observe an interconversion under CID conditions in the time scale of our IMS/IMS experiment, which validates that the peaks at t_d 20.7 and 22.1 ms are conformers of the same species. However, this interconversion does not occur to an extent that would make it the driving phenomenon for the observation of the major feature at 20.7 ms in the IMS profile of fragment from compound ③. One hypothesis is that, instead of an interconversion, the two conformers would arise from the coordination of the Li_+ cation in the parent trisaccharide.

Theoretical Study of the Conformational Space of the Li-Adducted Man-(α1,6)-Man Moiety. To evaluate this hypothesis, we opted to study the coordination of Li_+ with (***α***1,6)-mannobiose with quantum mechanical modeling. We thus performed Molecular Dynamics (MD) at the PM7 level of theory on both the ***α***- and ***β***-reducing end anomers of this disaccharide, the main advantage of this semiempirical exploration being to rapidly generate a high number of different conformations.

To explore the conformations generated by MD, we focused on basic geometric criteria related to our hypothesis that the conformers were related to Li_+ coordination. More specifically, we elected the distances between the Li atom and the intracyclic oxygen atoms of each Man residue (herein coined the ONR for the nonreducing end and the OR for the reducing end). Indeed, these distances efficiently reflect the distance of Li to the corresponding heterocycles.

For the ***α***-anomer (Figure 7A,B), we identified four conformational families by focusing on conformations for which Li was close to either the ONR or OR. The conformers in each of those families had energies ranging from −410 to −380 kcal/mol, therefore making them energetically indistinguishable given the uncertainty of the PM7 energy calculations (*ca.* 10−20 kcal/mol). The four theoretical families represented 2963 out of the 4133 total conformations generated by MD. For two of these families, in red (899 conformations) and blue (647 conformations), Li was located relatively close to both OR and ONR indicating compact structures. Aside from that, we also observed a family for which

Li was located at the nonreducing end (violet, 709 conformations), and a family for which Li was located at the reducing end (cyan, 708 conformations). For the *β*-anomer (Figure 7C,D), we observed the same families, but the contribution of the red, violet, and cyan families was significantly lower in favor of the blue family, which alone represented 1112 out of 4180 total conformations.
Next, we proceeded to a more in-depth analysis of the generated conformations. Representative structures for the four conformational families are presented in Figure 7E, exemplified on the *α*-anomer that is the most abundant for mannose in actual analytical conditions (additional structures are also shown in Figure S18). This confirmed that Li was placed at the nonreducing end for the violet population, between the two cycles for the red and blue populations, and at the reducing end for the cyan population.

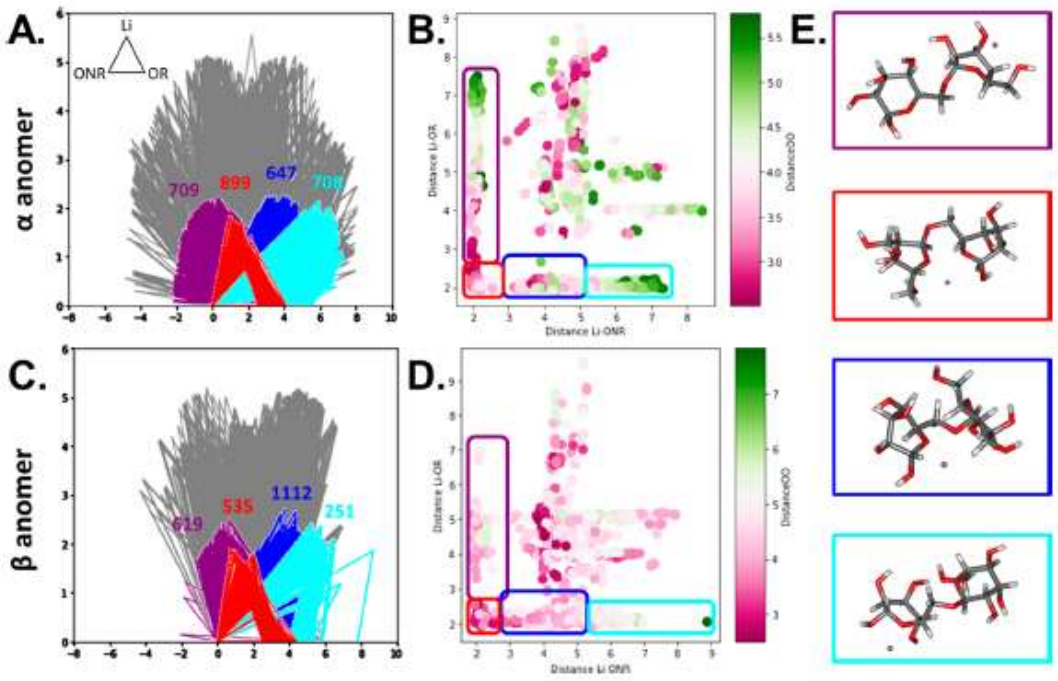

Figure 7. Geometric analysis of the Man-(*α*1,6)-Man conformations generated by Molecular Dynamics (MD) for both the *α* and *β* reducing-end anomers (A–B) and (C–D), respectively). The structures were analyzed by comparing the distances of the Li counterion with the intracyclic oxygens from the nonreducing Man (ONR) and from the reducing Man (OR). Two representations are proposed: in the first one (A and C), each conformation is represented by a triangle representing the distances between Li, the ONR, and the OR (in Å, anchored at the ONR = 0). The second one (B and D) presents the distance between Li and the ONR (*x*-axis) versus the distance Li-OR (*y*-axis), with the distance of the ONR-OR as a color scale. In E, representative structures for each identified population (exemplified on the *α* anomer) are shown.

In an attempt to correlate the conformational families of (*α*1,6)-mannobiose to the conformers that we observed in the DTD of the Y_2 fragment of trisaccharide ③, we performed (i) a calibration of the DTD to give an experimental $_{TW}CCS_{N2}$ distribution (CCSD) and (ii) theoretical CCS calculations for

the four representative structures using the trajectory method as implemented in ImoS v1.10 (the trajectory was calculated with the Verlet algorithm, using Lennard-Jones 4−6−12 potential). Since we observed that there were actually two peaks under the feature at t_d 20.7 ms (see Figure 6), we allowed for more peak overlap when fitting Gaussian under the CCSD compared to the earlier part of this paper. These results are presented in Figure 8.

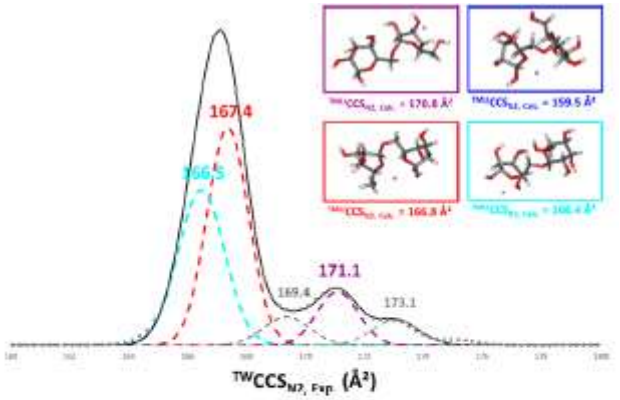

Figure 8. Comparison between the experimental CCS distribution of the m/z 351 fragment from trisaccharide ③ ($^{TW}CCS_{N2}$), and theoretical CCS for the four model conformations of Man-(α1,6)-Man (see Figure 7) calculated with the trajectory method (4−6−12 Lennard-Jones-induced dipole model, $^{TM(LJ}CCS_{N2}$). Three of the theoretical conformations were observed in the experimental spectrum (those framed in cyan, red, and purple).

Of note, we obtained very close experimental and theoretical CCS values, leading us to think that the following results are valid despite CCS errors being reported in the range of 1−2% for both CCS calibrations in TWIMS and theoretical CCS values.[55] However, the lower error when calculating the actual drift time for extended ion path length on the Cyclic, combined with the accuracy of conformation determination by MD methods, should compensate in part for this error. In the experimental distribution, the expected conformer of the Y_2 fragment (i.e., corresponding to the "normal" conformation of (α1,6)-mannobiose) was measured at ~171 A_2 (purple), while two peaks were fitted under the major feature at ~166.5 and 167.5 A_2 (cyan and red). The fourth configuration, theoretically calculated at 159.5 A_2 (blue), was not observed in the experimental spectrum. When compared to our theoretical calculations, this suggests that the expected value corresponds to the Li^+ being located at the nonreducing end (calcd 171 A_2), while the more compact ion populations correspond to Li^+ being located either at the reducing end or

between the two cycles.

Considering all of these results, we can explain the unexpected distribution of the Y_2 fragment of trisaccharide ③ as such: The normal cationization site of (*α*1,6)-mannobiose is located at the nonreducing end, which is occupied by a Gal*f* residue in the case of trisaccharide ③ causing Li^+ to coordinate with other sites instead. The precursor trisaccharide could therefore adopt different conformations at the Man-Man subunits compared to the reference Man-(*α*1,6)-Man. The different conformational states in the parent trisaccharide ③ would be preserved upon CID because the time scale of the experiment does not allow significant conformational changes back to the most stable conformer. Interestingly, we did not observe the occurrence of Man-Man conformers (or Gal*f* migration) when studying trisaccharide ⑤ (Gal*f* branched directly on the reducing Man with a free nonreducing Man) or trisaccharide ④ (Gal*p* analogue of trisaccharide ③). This indicates that the observed phenomenon is related both the Gal*f* subunit itself and its branching in the trisaccharide. Further computational studies at the trisaccharide level will be required to fully uncover the reaction mechanism behind the collisional dissociation of trisaccharide ③.

CONCLUSION

Overall, the present study shows that (i) disaccharidic fragments of $(Gal)_1(Man)_2$ trisaccharides matched well with the corresponding Gal-Man and Man-Man disaccharides in most cases, including Gal*f*-containing ones, but that (ii) in some cases the presence of the Gal*f* residue can impact the conformation of the entire oligosaccharide by modifying its coordination with the Li^+ countercation.

Importantly, we also observed a very probable Gal*f* migration to the reducing Man of a Gal*f*-(*β*1,4)-Man*p*-(*α*1,6)-Man*p* trisaccharide, which had not been previously reported. We note that this rearrangement occurred specifically on the same compound for which we observed a compaction, as attested by a shorter drift time. One hypothesis could be that a compaction around Li^+ would bring the nonreducing Gal*f* close to the reducing Man. The Gal*f*-(*β*1,4)-Man*p* bond likely fragile; this would allow the residue to migrate under the

effect of collisional activation.

ASSOCIATED CONTENT

***** Supporting Information

The Supporting Information is available free of charge at https://pubs.acs.org/doi/10.1021/jasms.2c00333. Synthesis and NMR validation of the mannobiose standards; instrumental conditions for cIMS analysis; HPLC analytical conditions; description of IMS_n strategies; LC-(IMS)-MS results for all oligosaccharides; Reference Drift Time values for our entire database of disaccharides; MS_3 spectrum of the unknown peak at *m/z* 351/t_d 20.7 ms; CID-IMS results for $[③+Na]_+$ and $[③-SPh+Li]_+$; IMS profile of (α1,6)-mannobiose under different activation conditions (PDF)

AUTHOR INFORMATION

Corresponding Author

David Ropartz – *INRAE, UR BIA, F-44316 Nantes, France; INRAE, PROBE Research Infrastructure, BIBS Facility, F-44316 Nantes, France;* orcid.org/0000-0003-4767-6940; Email: david.ropartz@inrae.fr

Authors

Simon Ollivier – *INRAE, UR BIA, F-44316 Nantes, France; INRAE, PROBE Research Infrastructure, BIBS Facility, F-44316 Nantes, France;* orcid.org/0000-0002-7671-1736

Laurent Legentil – *Univ Rennes, Ecole Nationale Supérieure de Chimie de Rennes, CNRS ISCR-UMR 6226, F-35000 Rennes, France;* orcid.org/0000-0003-1402-150X

Oznur Yeni – *Univ Lyon, Université Claude Bernard Lyon 1, CNRS, Institut Lumie`re Matie`re, F-69622 Villeurbanne, France*

Louis-Philippe David – *Univ Rennes, Ecole Nationale Supérieure de Chimie de Rennes, CNRS ISCR-UMR 6226, F-35000 Rennes, France*

Vincent Ferrie`res – *Univ Rennes, Ecole Nationale Supérieure de Chimie de Rennes, CNRS ISCR-UMR 6226, F-35000 Rennes, France;* orcid.org/0000-0002-2780-7774

Isabelle Compagnon – *Univ Lyon, Université Claude Bernard Lyon 1, CNRS, Institut Lumie`re Matie`re, F-69622 Villeurbanne, France;* orcid.org/0000-0003-2994-3961

Hélè`ne Rogniaux – *INRAE, UR BIA, F-44316 Nantes,*

France; INRAE, PROBE Research Infrastructure, BIBS Facility, F-44316 Nantes, France; orcid.org/0000-0001-6083-2034

Complete contact information is available at: https://pubs.acs.org/10.1021/jasms.2c00333

Author Contributions

S.O., H.R., and D.R. designed the IMS experiments. S.O. performed the IMS experiments. L.L, L.-P.D., and V.F. synthesized the oligosaccharides. O.Y. and I.C. performed the MD calculations. The manuscript was written through contributions of all authors. All authors have given approval to the final version of the manuscript.

Notes

The authors declare no competing financial interest.

ACKNOWLEDGMENTS

The authors thank the French National Research Agency for funding the ALGAIMS project (grant ANR-18-CE29-0006, https://algaims-35.webself.net/).

REFERENCES

(1) Taha, H. A.; Richards, M. R.; Lowary, T. L. Conformational Analysis of Furanoside-Containing Mono- and Oligosaccharides. *Chem. Rev.* 2013, *113* (3), 1851−1876.

(2) Peltier, P.; Euzen, R.; Daniellou, R.; Nugier-Chauvin, C.; Ferrie`res, V. Recent Knowledge and Innovations Related to Hexofuranosides: Structure, Synthesis and Applications. *Carbohydr. Res.* 2008, *343* (12), 1897−1923.

(3) Ferrie`res, V.; Nugier-Chauvin, C.; Legentil, L.; Tranchimand, S. Chapter 19: How Recent Knowledge on Furano-Specific Enzymes Has Renewed Interest for the Synthesis of Glycofuranosyl-Containing Conjugates. *Carbohydrate Chemistry* 2014, *40*, 401−417.

(4) Favreau, B.; Yeni, O.; Ollivier, S.; Boustie, J.; Le Devehat, F.; Guegan, J.-P.; Fanuel, M.; Rogniaux, H.; Bredy, R.; Compagnon, I.; Ropartz, D.; Legentil, L.; Ferrie`res, V. Synthesis of an Exhaustive Library of Naturally Occurring Galf-Manp and Galp-Manp Disaccharides. Toward Fingerprinting According to Ring Size by Advanced Mass Spectrometry-Based IM-MS and IRMPD. *J. Org. Chem.* 2021, *86*, 6390−6405.

(5) Manz, C.; Pagel, K. Glycan Analysis by Ion Mobility-Mass Spectrometry and Gas-Phase Spectroscopy. *Curr. Opin. Chem. Biol.* 2018, *42*, 16−24.

(6) Hofmann, J.; Pagel, K. Glycan Analysis by Ion Mobility-Mass Spectrometry. *Angew. Chem.-Int. Ed.* 2017, *56* (29), 8342–8349.
(7) Miller, R. L.; Guimond, S. E.; Schworer, R.; Zubkova, O. V.; Tyler, P. C.; Xu, Y.; Liu, J.; Chopra, P.; Boons, G.-J.; Grabarics, M.; Manz, C.; Hofmann, J.; Karlsson, N. G.; Turnbull, J. E.; Struwe, W. B.; Pagel, K. Shotgun Ion Mobility Mass Spectrometry Sequencing of Heparan Sulfate Saccharides. *Nat. Commun.* 2020, *11* (1), 1–12.
(8) Huang, Y.; Dodds, E. D. Ion Mobility Studies of Carbohydrates as Group I Adducts: Isomer Specific Collisional Cross Section Dependence on Metal Ion Radius. *Anal. Chem.* 2013, *85* (20), 9728–9735.
(9) Huang, Y. T.; Dodds, E. D. Discrimination of Isomeric Carbohydrates as the Electron Transfer Products of Group II Cation Adducts by Ion Mobility Spectrometry and Tandem Mass Spectrometry. *Anal. Chem.* 2015, *87* (11), 5664–5668.
(10) Gray, C. J.; Schindler, B.; Migas, L. G.; Picˇmanova, M.; Allouche, A. R.; Green, A. P.; Mandal, S.; Motawia, M. S.; Sanchez-Perez, R.; Bjarnholt, N.; Moller, B. L.; Rijs, A. M.; Barran, P. E.; Compagnon, I.; Eyers, C. E.; Flitsch, S. L. Bottom-Up Elucidation of Glycosidic Bond Stereochemistry. *Anal. Chem.* 2017, *89* (8), 4540–4549.
(11) Pagel, K.; Harvey, D. J. Ion Mobility-Mass Spectrometry of Complex Carbohydrates: Collision Cross Sections of Sodiated NLinked Glycans. *Anal. Chem.* 2013, *85* (10), 5138–5145.
(12) Ujma, J.; Ropartz, D.; Giles, K.; Richardson, K.; Langridge, D.; Wildgoose, J.; Green, M.; Pringle, S. Cyclic Ion Mobility Mass Spectrometry Distinguishes Anomers and Open-Ring Forms of Pentasaccharides. *J. Am. Soc. Mass Spectrom.* 2019, *30* (6), 1028–1037.
(13) Ropartz, D.; Fanuel, M.; Ujma, J.; Palmer, M.; Giles, K.; Rogniaux, H. Structure Determination of Large Isomeric Oligosaccharides of Natural Origin through Multipass and Multistage Cyclic Traveling-Wave Ion Mobility Mass Spectrometry. *Anal. Chem.* 2019, *91* (18), 12030–12037.
(14) Ollivier, S.; Tarquis, L.; Fanuel, M.; Li, A.; Durand, J.; Laville, E.; Potocki-Veronese, G.; Ropartz, D.; Rogniaux, H. Anomeric Retention of Carbohydrates in Multistage Cyclic Ion Mobility (IMSn): De Novo Structural Elucidation of Enzymatically Produced Mannosides. *Anal. Chem.* 2021, *93* (15), 6254–6261.
(15) Ollivier, S.; Fanuel, M.; Rogniaux, H.; Ropartz, D. Molecular Networking of High-Resolution Tandem Ion Mobility Spectra: A Structurally Relevant Way of Organizing Data in Glycomics? *Anal. Chem.* 2021, *93* (31), 10871–10878.
(16) Ropartz, D.; Fanuel, M.; Ollivier, S.; Lissarrague, A.; Benkoulouche, M.; Mulard, L. A.; Andre, I.; Guieysse, D.; Rogniaux, H. Combination of High-Resolution Multistage Ion

Mobility and Tandem MS with High Energy of Activation to Resolve the Structure of Complex Chemoenzymatically Synthesized Glycans. *Anal. Chem.* 2022, *94* (4), 2279−2287.
(17) Li, H. L.; Bendiak, B.; Siems, W. F.; Gang, D. R.; Hill, H. H. Carbohydrate Structure Characterization by Tandem Ion Mobility Mass Spectrometry (IMMS)(2). *Anal. Chem.* 2013, *85* (5), 2760−2769.
(18) Barnes, L.; Schindler, B.; Chambert, S.; Allouche, A. R.; Compagnon, I. Conformational Preferences of Protonated NAcetylated Hexosamines Probed by InfraRed Multiple Photon Dissociation (IRMPD) Spectroscopy and Ab Initio Calculations. *Int. J. Mass Spectrom.* 2017, *421*, 116−123.
(19) Barnes, L.; Allouche, A.-R.; Chambert, S.; Schindler, B.; Compagnon, I. Ion Spectroscopy of Heterogeneous Mixtures: IRMPD and DFT Analysis of Anomers and Conformers of Monosaccharides. *Int. J. Mass Spectrom.* 2020, *447*, 116235.
(20) Depraz Depland, A.; Renois-Predelus, G.; Schindler, B.; Compagnon, I. Identification of Sialic Acid Linkage Isomers in Glycans Using Coupled InfraRed Multiple Photon Dissociation (IRMPD) Spectroscopy and Mass Spectrometry. *Int. J. Mass Spectrom.* 2018, *434*, 65−69.
(21) Schindler, B.; Barnes, L.; Gray, C. J.; Chambert, S.; Flitsch, S. L.; Oomens, J.; Daniel, R.; Allouche, A. R.; Compagnon, I. IRMPD Spectroscopy Sheds New (Infrared) Light on the Sulfate Pattern of Carbohydrates. *J. Phys. Chem. A* 2017, *121* (10), 2114−2120.
(22) Yeni, O.; Schindler, B.; Moge, B.; Compagnon, I. Rapid IRMPD (InfraRed Multiple Photon Dissociation) Analysis for Glycomics. *Analyst* 2022, *147*, 312.
(23) Yeni, O.; Gharbi, A.; Chambert, S.; Rouillon, J.; Allouche, A.-R.; Schindler, B.; Compagnon, I. O-Acetylated Sugars in the Gas Phase: Stability, Migration, Positional Isomers and Conformation. *Phys. Chem. Chem. Phys.* 2022, *24* (2), 1016−1022.
(24) Schindler, B.; Legentil, L.; Allouche, A. R.; Ferrieres, V.; Compagnon, I. Spectroscopic Diagnostic for the Ring-Size of Carbohydrates in the Gas Phase: Furanose and Pyranose Forms of GalNAc. *Phys. Chem. Chem. Phys.* 2019, *21* (23), 12460−12467.
(25) Ho, J. S.; Gharbi, A.; Schindler, B.; Yeni, O.; Bredy, R.; Legentil, L.; Ferrie`res, V.; Kiessling, L. L.; Compagnon, I. Distinguishing Galactoside Isomers with Mass Spectrometry and Gas-Phase Infrared Spectroscopy. *J. Am. Chem. Soc.* 2021, *143*, 10509.
(26) Gabelica, V.; Marklund, E. Fundamentals of Ion Mobility Spectrometry. *Curr. Opin. Chem. Biol.* 2018, *42*, 51−59.
(27) Gabelica, V.; Shvartsburg, A. A.; Afonso, C.; Barran, P.; Benesch, J. L. P.; Bleiholder, C.; Bowers, M. T.; Bilbao, A.; Bush, M. F.; Campbell, J. L.; Campuzano, I. D. G.; Causon, T.; Clowers, B. H.; Creaser, C. S.; De Pauw, E.; Far, J.; Fernandez-Lima, F.; Fjeldsted, J.

C.; Giles, K.; Groessl, M.; Hogan Jr, C. J.; Hann, S.; Kim, H. I.; Kurulugama, R. T.; May, J. C.; McLean, J. A.; Pagel, K.; Richardson, K.; Ridgeway, M. E.; Rosu, F.; Sobott, F.; Thalassinos, K.; Valentine, S. J.; Wyttenbach, T. Recommendations for Reporting Ion Mobility Mass Spectrometry Measurements. *Mass Spectrom. Rev.* 2019, *38* (3), 291–320.
(28) Gabelica, V. CHAPTER 1:Ion Mobility-Mass Spectrometry: An Overview. *Ion Mobility-Mass Spectrometry* 2021, 1–25.
(29) Giles, K.; Ujma, J.; Wildgoose, J.; Pringle, S.; Richardson, K.; Langridge, D.; Green, M. A Cyclic Ion Mobility-Mass Spectrometry System. *Anal. Chem.* 2019, *91* (13), 8564–8573.
(30) Deng, L. L.; Webb, I. K.; Garimella, S. V. B.; Hamid, A. M.; Zheng, X. Y.; Norheim, R. V.; Prost, S. A.; Anderson, G. A.; Sandoval, J. A.; Baker, E. S.; Ibrahim, Y. M.; Smith, R. D. Serpentine Ultralong Path with Extended Routing (SUPER) High Resolution Traveling Wave Ion Mobility-MS Using Structures for Lossless Ion Manipulations. *Anal. Chem.* 2017, *89* (8), 4628–4634.
(31) Gorin, P. A. J.; Iacomini, M. Structural Diversity of D-Galactod-Mannan Components Isolated from Lichens Having Ascomycetous Mycosymbionts. *Carbohydr. Res.* 1985, *142* (2), 253–267.
(32) Iacomini, M.; Schneider, C. L.; Gorin, P. A. J. Comparative Studies on the Polysaccharides of Cladonia Alpestris (Reindeer Moss), Cladonia Confusa, and Cladonia Amaurocraea. *Carbohydr. Res.* 1985, *142* (2), 237–251.
(33) Carbonero, E. R.; Smiderle, F. R.; Gracher, A. H. P.; Mellinger, C. G.; Torri, G.; Ahti, T.; Gorin, P. A. J.; Iacomini, M. Structure of Two Glucans and a Galactofuranomannan from the Lichen Umbilicaria Mammulata. *Carbohydr. Polym.* 2006, *63* (1), 13–18.
(34) Omarsdottir, S.; Petersen, B. O.; Paulsen, B. S.; Togola, A.; Duus, J. O.; Olafsdottir, E. S. Structural Characterisation of Novel Lichen Heteroglycans by NMR Spectroscopy and Methylation Analysis. *Carbohydr. Res.* 2006, *341* (14), 2449–2455.
(35) Omarsdottir, S.; Freysdottir, J.; Olafsdottir, E. S. Immunomodulating Polysaccharides from the Lichen Thamnolia Vermicularis Var. Subuliformis. *Phytomedicine* 2007, *14* (2), 179–184.
(36) Williamson, D. L.; Bergman, A. E.; Nagy, G. Investigating the Structure of *α*/*β* Carbohydrate Linkage Isomers as a Function of Group I Metal Adduction and Degree of Polymerization as Revealed by Cyclic Ion Mobility Separations. *J. Am. Soc. Mass Spectrom.* 2021, *32* (10), 2573–2582.
(37) Kailemia, M. J.; Ruhaak, L. R.; Lebrilla, C. B.; Amster, I. J. Oligosaccharide Analysis by Mass Spectrometry: A Review of Recent Developments. *Anal. Chem.* 2014, *86* (1), 196–212.
(38) Hofmeister, G. E.; Zhou, Z.; Leary, J. A. Linkage Position Determination in Lithium-Cationized Disaccharides: Tandem Mass

Spectrometry and Semiempirical Calculations. *J. Am. Chem. Soc.* 1991, *113* (16), 5964–5970.
(39) Tsai, S.-T.; Chen, J.-L.; Ni, C.-K. Does Low-Energy Collision-Induced Dissociation of Lithiated and Sodiated Carbohydrates Always Occur at Anomeric Carbon of the Reducing End? *Rapid Commun. Mass Spectrom.* 2017, *31* (21), 1835–1844.
(40) Bythell, B. J.; Abutokaikah, M. T.; Wagoner, A. R.; Guan, S.; Rabus, J. M. Cationized Carbohydrate Gas-Phase Fragmentation Chemistry. *J. Am. Soc. Mass Spectrom.* 2017, *28* (4), 688–703.
(41) Abutokaikah, M. T.; Frye, J. W.; Tschampel, J.; Rabus, J. M.; Bythell, B. J. Fragmentation Pathways of Lithiated Hexose Monosaccharides. *J. Am. Soc. Mass Spectrom.* 2018, *29* (8), 1627–1637.
(42) Chizhov, A. O.; Filatov, A. V.; Perepelov, A. V.; Knirel, Y. A. A New Example of Rearrangement Observed in the Tandem Mass Spectra of Oligosaccharides. *J. Anal. Chem.* 2020, *75* (14), 1842–1845.
(43) Guan, S.; Bythell, B. J. Evidence of Gas-Phase Pyranose-to-Furanose Isomerization in Protonated Peptidoglycans. *Phys. Chem. Chem. Phys.* 2021, *23* (40), 23256–23266.
(44) Rabus, J. M.; Guan, S.; Schultz, L. M.; Abutokaikah, M. T.; Maitre, P.; Bythell, B. J. Protonated *α*-N-Acetyl Galactose Glycopeptide Dissociation Chemistry. *J. Am. Soc. Mass Spectrom.* 2022, *33* (9), 1745–1752.
(45) Polasky, D. A.; Dixit, S. M.; Fantin, S. M.; Ruotolo, B. T. CIUSuite 2: Next-Generation Software for the Analysis of Gas-Phase Protein Unfolding Data. *Anal. Chem.* 2019, *91* (4), 3147–3155.
(46) Ruotolo, B. T.; Benesch, J. L. P.; Sandercock, A. M.; Hyung, S.-J.; Robinson, C. V. Ion Mobility-Mass Spectrometry Analysis of Large Protein Complexes. *Nat. Protoc.* 2008, *3* (7), 1139–1152.
(47) Bush, M. F.; Hall, Z.; Giles, K.; Hoyes, J.; Robinson, C. V.; Ruotolo, B. T. Collision Cross Sections of Proteins and Their Complexes: A Calibration Framework and Database for Gas-Phase Structural Biology. *Anal. Chem.* 2010, *82* (22), 9557–9565.
(48) Stewart, J. J. P. MOPAC2012. http://openmopac.net/.
(49) Nagy, G.; Attah, I. K.; Garimella, S. V. B.; Tang, K.; Ibrahim, Y. M.; Baker, E. S.; Smith, R. D. Unraveling the Isomeric Heterogeneity of Glycans: Ion Mobility Separations in Structures for Lossless Ion Manipulations. *Chem. Commun.* 2018, *54* (83), 11701–11704.
(50) Warnke, S.; Faleh, A. B.; Scutelnic, V.; Rizzo, T. R. Separation and Identification of Glycan Anomers Using Ultrahigh-Resolution Ion-Mobility Spectrometry and Cryogenic Ion Spectroscopy. *J. Am. Soc. Mass Spectrom.* 2019, *30* (11), 2204–2211.
(51) Domon, B.; Costello, C. E. A Systematic Nomenclature for Carbohydrate Fragmentations in FAB-MS MS Spectra of Glycoconjugates.

Glycoconjugate J. 1988, *5* (4), 397–409.
(52) Campbell, M. T.; Chen, D.; Glish, G. L. Identifying the DPentoses Using Water Adduction to Lithium Cationized Molecule. *J. Am. Soc. Mass Spectrom.* 2017, *28* (7), 1420–1424.
(53) Campbell, M. T.; Chen, D.; Wallbillich, N. J.; Glish, G. L. Distinguishing Biologically Relevant Hexoses by Water Adduction to the Lithium-Cationized Molecule. *Anal. Chem.* 2017, *89* (19), 10504–10510.
(54) Campbell, M. T.; Chen, D.; Glish, G. L. Distinguishing Linkage Position and Anomeric Configuration of Glucose-Glucose Disaccharides by Water Adduction to Lithiated Molecules. *Anal. Chem.* 2018, *90* (3), 2048–2054.
(55) Richardson, K.; Langridge, D.; Dixit, S. M.; Ruotolo, B. T. An Improved Calibration Approach for Traveling Wave Ion Mobility Spectrometry: Robust, High-Precision Collision Cross Sections. *Anal. Chem.* 2021, *93* (7), 3542–3550.